Published in final edited form as:
Cell Rep. 2014 November 6; 9(3): 1089–1098. doi:10.1016/j.celrep.2014.09.053.

Structure and Cancer Immunotherapy of the B7 Family Member B7x

Hyungjun Jeon[1,9], **Vladimir Vigdorovich**[1,5,9], **Sarah C. Garrett-Thomson**[2], **Murali Janakiram**[3], **Udupi A. Ramagopal**[2], **Yael M. Abadi**[1,6], **Jun Sik Lee**[1,7], **Lisa Scandiuzzi**[1], **Kim C Ohaegbulam**[1], **Jordan M Chinai**[1], **Ruihua Zhao**[1,8], **Yu Yao**[4], **Ying Mao**[4], **Joseph A. Sparano**[3], **Steven C. Almo**[2,*], and **Xingxing Zang**[1,3,*]

[1]Department of Microbiology and Immunology, Albert Einstein College of Medicine, Bronx, NY 10461, USA

[2]Department of Biochemistry, Physiology and Biophysics, Albert Einstein College of Medicine, Bronx, NY 10461, USA

[3]Department of Oncology, Montefiore Medical Center, Albert Einstein College of Medicine, Bronx, NY 10467, USA

[4]Department of Neurosurgery, Huashan Hospital, Fudan University, Shanghai 200040, China

SUMMARY

B7x (B7-H4 or B7S1) is a member of the B7 family that can inhibit T cell function. B7x protein is absent in most normal human tissues and immune cells, but is overexpressed in human cancers and often correlates with negative clinical outcome. The expression pattern and function of B7x suggest that it may be a potent immunosuppressive pathway in human cancers. Here we determined the crystal structure of human B7x IgV domain at 1.59Å resolution and mapped the epitopes recognized by monoclonal antibodies. We developed a new in vivo system to screen therapeutic monoclonal antibodies against B7x, and found that the clone 1H3 significantly inhibited growth of B7x-expressing tumor in vivo via multiple mechanisms. Furthermore, the surviving mice given 1H3 treatment were resistant to tumor re-challenge. Our data suggest that

*Correspondence: xing-xing.zang@einstein.yu.edu or steve.almo@einstein.yu.edu.
[5]Present address: Seattle BioMed, Seattle, WA 98109, USA
[6]Present address: Department of Neurology, Yale University School of Medicine, New Haven, CT 06510, USA
[7]Present address: Department of Biology, College of Natural Science, Chosun, University, Gwangju 501-759, South Korea.
[8]Present address: School of Life Science, Fudan University, Shanghai 200433, China
[9]These authors contributed equally to this work.

Other detailed experimental procedures can be found in the Supplemental Experimental Procedures.

AUTHOR CONTRIBUTIONS

H.J. performed experiments in immunotherapy. V.V. and U.A.R. determined the crystal structure, and V.V. performed the affinity measurements. S.C.G performed epitope mapping. M.J. performed immunohistochemistry experiments. Y.M.A. helped with several experiments. J.S.L. established cell lines. L.S., K.C.O., J.M.C., R.Z., Y.Y., Y.M. and J.A.S. provided invaluable reagents and advice on experiments. H.J. and V.V. analyzed the data and wrote the manuscript. X.Z. and S.C.A. supervised the study and wrote the manuscript. All authors read and approved the manuscript.

targeting B7x on tumors is a promising cancer immunotherapy and humanized 1H3 may be efficacious for immunotherapy of human cancers.

INTRODUCTION

T cell costimulation and coinhibition mediated by the B7 ligand family and the CD28 receptor family have crucial roles in modulating T cell activation, proliferation, and differentiation into effector function and memory generation (Greenwald et al., 2005; Zang and Allison, 2007). The B7-1/B7-2/CD28/CTLA-4 pathway is a well-characterized T cell costimulatory and coinhibitory pathway. A monoclonal antibody (mAb) against CTLA-4 was recently approved for treatment of metastatic melanoma (Hodi et al., 2010; Sharma et al., 2011) and CTLA-4-Ig fusion protein has been used to treat rheumatoid arthritis and to prevent acute kidney transplant rejection (Fiocco et al., 2008; Vincenti et al., 2011). The past decade has witnessed a new era in the discovery of other B7 and CD28 members and understanding of their immune regulation, including B7h/ICOS, PD-L1/PD-L2/PD-1, B7-H3/receptor, B7x/receptor and HHLA2 (B7y/B7-H5/B7h7)/TMIGD2 (CD28h) (Janakiram, 2014; Zhao et al., 2013; Zhu et al., 2013). mAbs against PD-1 and PD-L1 are currently in clinical trials with cancer patients (Brahmer et al., 2012; Topalian et al., 2012). Clearly, further studies of the less characterized B7/CD28 pathways will not only sharpen our understanding of the immune system but also lead to new therapies for a wide range of diseases.

B7x (B7-H4 or B7S1), a member of the B7 family, can inhibit T cell proliferation and cytokine production in vitro (Prasad et al., 2003; Sica et al., 2003; Zang et al., 2003). Recent works reveal that overexpression of B7x on pancreatic cells is sufficient to abolish CD4 or CD8 T cell-induced diabetes (Lee et al., 2012; Wei et al., 2011), demonstrating that manipulating of the B7x pathway can achieve significant functional consequences in vivo. In contrast to the expression pattern of B7-1 and B7-2, B7x protein is mainly detected in nonlymphoid organs (Hofmeyer et al., 2012; Lee et al., 2012; Tringler et al., 2005; Wei et al., 2011). One of the most intriguing characteristics of B7x is that it is overexpressed in numerous human cancers and, in many cases, correlates with negative clinical outcome (Barach et al., 2010; Janakiram et al., 2012; Zang and Allison, 2007). A large investigation of B7 family molecules in human malignancy demonstrated that prostate cancer patients with tumors that express B7x highly are more likely to have disease spread at the time of surgery, and are at an increased risk of cancer recurrence and cancer-specific death (Zang et al., 2007). In another study, 103 ovarian cancer samples tested express B7x(Zang et al., 2010). In contrast to tumor tissues, only scattered B7x-positive cells are detected in non-neoplastic ovarian tissues (Zang et al., 2010). In line with these results, others have reported that B7x overexpression can be seen in human cancers of the lung (Sun et al., 2006), breast (Tringler et al., 2005), kidney (Krambeck et al., 2006), pancreas (Awadallah et al., 2008), esophagus (Chen et al., 2011), skin (Quandt et al., 2011), and gut (Jiang et al., 2010). In renal cell carcinoma (Krambeck et al., 2006), patients with tumors expressing B7x are three times more likely to die from cancer compared to patients lacking B7x. In esophageal squamous cell carcinoma, expression levels of B7x on tumor cells are significantly correlated with distant metastasis, tumor stage and worse survival, and are inversely

correlated with densities of CD3 T cells in tumor nest and CD8 T cells in tumor stromal (Chen et al., 2011).

The overexpression of B7x by so many types of human cancers suggests that this pathway may be exploited as an important immune evasion mechanism. Here, we reported the first crystal structure of human B7x IgV domain and developed a new cancer immunotherapy using mAbs recognizing this domain. Our findings suggest that targeting B7x on tumors can be an innovative tumor immunotherapy.

RESULTS

Crystal Structure of Human B7x IgV Domain

Like other B7 family members, B7x possesses extracellular IgV and IgC domains (Prasad et al., 2003; Sica et al., 2003; Zang et al., 2003). The IgV domain has previously been characterized as the receptor-binding domain for B7-1 (Stamper et al., 2001), B7-2 (Schwartz et al., 2001), PD-L1 (Lin et al., 2008) and PD-L2 (Lazar-Molnar et al., 2008). Therefore, we sought to understand the structure of the B7x IgV domain (B7x-IgV) to inform future studies of its interaction with receptors and antibodies. Human and murine B7x sequences share ~90% sequence identity overall and in their IgV domains. The crystals of human B7x-IgV exhibited diffraction consistent with the space group $P4_32_12$ (a = 46.5 Å, b = 46.5 Å, c = 115.77 Å; one molecule per asymmetric unit), and extended to 1.59 Å (Table 1). The final model consists of residues 35–148, which are organized into a β-sandwich composed of sheets ABED (back-sheet; light blue) and C´´C´CFG (front-sheet; light green) (Figure 1A). The sequence of the human B7x-IgV is predicted to contain a single glycosylation site at Asn112, and we observed a region of well-defined electron density near this position consistent with the presence of corresponding to 5 sugar residues of a branched glycan (Figure 1B). Superposition of B7x and PD-L1 IgV domains (Figure 1C) resulted in an root-mean-square deviation of 1.327 Å with differences apparent largely in the loop regions, demonstrating that the fold is highly conserved between these two B7 family members.

Interaction of mAbs with B7x IgV Domain

We recently generated B7x-specific mAbs from B7x−/− mice(Wei et al., 2011). mAbs 1H3 (IgG1) and 12D11 (IgG1) bound human or mouse B7x but not other B7 family members (Figure S1A). We estimated the binding rate constants and derived the corresponding equilibrium dissociation constants (K_D's) for the interactions of mAbs with recombinant murine B7x ectodomain, as well as murine and human B7x IgV through surface plasmon resonance (SPR). In these experiments, purified antibodies were immobilized on the biosensor surface and recombinant protein samples at various concentrations were injected for 120–240s followed by dissociation in running buffer. mAbs 1H3, 12D11 and 15D12 strongly interacted with all of these proteins with dissociation constants summarized in Table 2. Representative sensorgrams are shown in Figure S1B.

Mapping the Epitopes in Human B7x IgV Domain Recognized by 1H3 and 12D11

To define the epitope recognized by 1H3 and 12D11, we generated a series of B7x point mutants and measured their effect on binding of 1H3 and 12D11. Both antibodies showed a similar pattern of binding to B7x except in the case of the I62A mutant. Mutations at residues E59, I62, K63, E74, K84, F104, D106, Q107 and S135 resulted in greater than 40% loss of antibody binding (Figure 1D and Figure S1C) even though their overall expression was similar to wild-type B7x. These observations suggest that perturbation of these residues did not cause global B7x misfolding or instability and that the effects on antibody binding were the result of impaired/unfavorable interactions at the binding interface. Clustering of the identified residues on the surface of the B7x IgV domain further suggests that the observed effects on antibody binding were not due to non-specific effects on overall structure or stability of B7x.

Anti-B7x mAb therapy in mouse B7x-expressing tumor models

Although B7x is over-expressed in many human cancers (Jeon et al., 2013), it is lost rapidly in vitro culture (Dangaj et al., 2013). We found that most human and mouse tumor cell lines were B7x protein negative. To develop a functional screening system for immunotherapy, we first established tumor cell lines that stably express cell surface B7x using a retroviral expression vector transfection. (Figure S2A and S2B). The B7x expression level on CT26 cells was comparable to the expression levels of B7x on human cancer cell lines such as MCF-7, MDA-MB-468 and SK-BR-3 (Figure S2C–E). Mouse colon carcinoma CT26 and murine and human B7x/CT26 were intravenously (iv) injected into syngeneic BALB/c mice to induce experimental lung metastasis. The average number of lung tumor nodules in murine and human B7x/CT26 group was ~3.5 fold higher than that in the CT26 group (Figure S2F). In line with this result, B7x/CT26 injected mice had a lower survival rate compared to mice receiving naïve CT26 cells (Figure S2G). These results demonstrate that B7x overexpression on a murine tumor cell line, like on human tumors, correlates with worse outcomes.

We next screened the in vivo therapeutic effect of B7x-specific mAbs in the B7x/CT26-induced pulmonary metastasis model. B7x/CT26 cells were iv injected into BALB/c mice followed by intraperitoneal (ip) injection of anti-B7x mAbs. On day 17, lung tumor nodules were examined. We found that two mAbs, 1H3 and 12D11, significantly reduced ~60% of tumor nodules in lungs (Figure 2A). The 4T1 murine tumor model is a widely-used model in which the cancerous cells spontaneously metastasize to the lung(Aslakson and Miller, 1992). We then decided to validate the efficacy of 1H3 in the murine B7x/4T1 primary tumor model (Figure S2H). 1H3 treatment significantly suppressed primary tumor growth and efficiently reduced primary tumor-induced metastatic tumor nodules in the lung (Figure 2B and Figure S4B). These results from two tumor models suggest that anti-B7x markedly reduces tumor nodules in lungs.

Anti-B7x mAb Therapy in a Human B7x-expressing Tumor Model

B7x is very evolutionally conserved (Prasad et al., 2003; Sica et al., 2003; Zang et al., 2003), and mature B7x protein shares 90% amino acid identity in the extracellular domains between human and mice. Since both 1H3 and 12D11 recognized human B7x (Table 2), we

wanted to test the therapeutic effects of these two mAbs in a human B7x-expressing tumor model in vivo. Like mouse B7x, the expression of human B7x on CT26 markedly increased tumor nodules in the lung (Figure S2F). We then examined the effect of mAbs on hB7x/CT26 in vivo. Mice were iv injected with hB7x/CT26 and then treated with 1H3 or 12D11. On day 17, the average numbers of lung tumor nodules in 1H3-treated and 12D11-treated groups were 97 and 236, respectively, whereas the number in the control group was 251 (Figure 2C). Because proteins in the tumor microenvironments can be modified by post-translational modifications such as glycosylation and phosphorlyation, we questioned whether 1H3 recognized human B7x that is naturally expressed in human tumors. Using immunohistochemical staining, we found that 1H3 recognized nature B7x in various human cancers from the colon, ovary, skin, lung, breast, liver, nasal cavity, and stomach (Figure 2D). These results suggest that human B7x promotes tumor growth in vivo and that mAb 1H3 recognizes human B7x and inhibits progression of these tumors in vivo. As 1H3 was the only mAb that inhibited both human and mouse B7x-mediated tumor progression, we used it for the subsequent experiments.

1H3 mAb-treated Mice Survive Tumor Rechallenge

We next investigated the effect of 1H3 on the survival of mice bearing B7x/CT26 tumor. In agreement with the lung tumor nodule results, 1H3 treated mice had a significant lower mortality than did control IgG treated mice. By day 60, post injection of tumor, 100% of IgG-treated mice were dead, whereas only 50% of 1H3-treated mice had died (Figure 3A). These surviving mice appeared to be healthy. We then examined whether the surviving mice had resistance to the tumor rechallenge. These mice were rechallenged with the same number of B7x/CT26 cells, and all of them remained alive. On day 120, mice were sacrificed and their lungs were free of visible tumor nodules. Furthermore, HE staining of lung sections from these mice showed free of cancerous cells (Figure 3B).

Anti-B7x Therapy Increases Infiltrating T and NK Cells and Decreases Infiltrating MDSCs in Tumors

To dissect the therapeutic mechanisms of 1H3 treatment, we prepared single-cell suspensions from tumor-bearing lungs and analyzed the immune cells by flow cytometry. 1H3-treated mice had significantly higher percentage of CD45+ immune cell infiltrate than control IgG-treated mice (Figure 4A). Among these CD45+ cells, the 1H3 treatment strongly increased tumor infiltrates of CD8 T cells and NK cells (Figure 4B), two major types of anti-tumor immune cells. We used SPSYVYHQF/H-2L^{d} tetramer to detect CD8 T cells specific for CT26 tumor antigen epitope AH1 (amino acids 423–431 SPSYVYHQF) (Huang et al., 1996). In agreement with the increased total CD8 T cells, 1H3 treatment increased the percentage of AH1-specific CD8 T cells (Figure 4C). In addition, we found that the percentage of AH1-specific CD8 T cells in blood was reduced in 1H3 treated mice (Figure 4D), but the percentage of tumor-associated macrophages in blood was not changed by 1H3 treatment (Figure S3A). There were no significant changes of AH1-specific CD8 T cells and tumor-associated macrophages in spleens. These results suggest that 1H3 treatment facilitated the migration of tumor specific CD8 T cells from blood to tumor bearing lungs. Recent studies identified the co-expression of Tim-3 and PD-1 (Tim-3+PD-1+) cells as a unique phenotype of exhausted CD8 or CD4 T cells in melanoma and leukemia (Fourcade et

al., 2010; Goding et al., 2013; Zhou et al., 2011). Therefore, we examined the effect of 1H3 on these two inhibitory receptors on T cells. We found that 1H3-treated mice had significantly fewer CD4 T cells that were Tim-3+PD-1+, Tim-3+ alone and PD-1+ alone relative to those of control mice (Figure 4E). These results suggest that 1H3 treatment reduced the conversion of CD4 T cells from an activated to an exhausted state. Along with these finding, the 1H3 treatment enhanced CD4 T cells to produce IFN-γ (Figure 4F), a critical cytokine for anti-tumor immunity. Perforin and granzyme B are effector molecules in CD8 T cells and NK cells that mediate tumor cell death. We found that 1H3 treatment increased their production in CD8 T cells and NK cells although the difference did not reach statistical significance (Figure S3B and S3C). In the tumor microenvironment, suppression of effector T cell function is often driven by immunosuppressive cells. Therefore, we investigated the effect of 1H3 treatment on immunosuppressive cell infiltrates in tumor bearing lungs. We found that the treatment did not change the percentage of Foxp3+CD4+ regulatory T cells (Tregs) (Figure S3D), but did reduce CD11b+Ly6C+ monocytic myeloid-derived suppressor cells (MDSCs) infiltrating tumor (Figure 4G). The combined increase of CD8 T cells, NK and IFN-γ-producing CD4 T cells along with the reduction of MDSCs in the 1H3 treatment collectively create an environment with a lower ratio of suppressive cells to anti-tumor effector cells (Figure 4H).

Effect of Anti-B7x Therapy on the Tumor Microenvironment

VEGF from tumor cells, stromal cells and immune cells stimulates angiogenesis in tumor microenvironment. This angiogenesis facilitates tumor growth and metastasis (Roda et al., 2012; Roland et al., 2009). We found that the VEGF concentration in tumor-bearing lungs from 1H3 treated mice was significantly lower than that of control mice (Figure 4I). The 1H3 treatment also lowered the concentration of TGF-β in tumor-bearing lungs (Figure 4J), one of the key cytokines responsible for suppressing anti-tumor immunity (Fridlender et al., 2009).

1H3 Kills Tumor Cells Through ADCC

Antibodies can eliminate virus-infected cells or tumor cells via antibody-dependent cellular cytotoxicity (ADCC) (Clynes et al., 2000; Isitman et al., 2012; Kohrt et al., 2012), a mechanism requiring antibody, antigen-expressed target cells and effector cells expressing Fc receptors. We examined whether 1H3 was able to kill tumor cells expressing B7x or tumor cells without expressing B7x through ADCC. We found that 1H3 induced 50% more target cells death compared to control IgG (Figure 5A and Figure S4A).

1H3 Partially Blocks B7x-mediated T Cell Coinhibition

It has been demonstrated that B7x inhibits T cell function in the presence of TCR signaling in vitro (Prasad et al., 2003; Sica et al., 2003; Zang et al., 2003), but the receptor expressed on activated T cells is currently unknown. We next questioned whether 1H3 could inhibit B7x-mediated T cell coinhibition using a system modified from our previous studies (Zang et al., 2003). As expected, T cells proliferated vigorously when incubated with anti-CD3 and control Ig with more than 73% of T cells dividing. When T cells were incubated with anti-CD3 and B7x-Ig, significantly fewer T cells proliferated, with about 41% dividing. The presence of 1H3 in the system significantly neutralized B7x-mediated T cell coinhibition, as

1H3 increased T cell proliferation to >61%. Furthermore, the Fab fragment of 1H3 had a similar neutralizing effect on B7x-induced T cell coinhibition (Figure 5B). These results reveal that 1H3 can partially block B7x-mediated T cell coinhibition. To assess whether 1H3 therapy depends on ADCC and/or functional neutralization in vivo, we compared the therapeutic efficacies of 1H3 and its Fab, which cannot mediate ADCC. Mice treated with the Fab had significantly fewer lung tumor nodules than did mice treated with control IgG, but had significantly more lung tumor nodules than did mice treated with 1H3 (Figure 5C). To confirm this effect, we validated the efficacy of 1H3 and Fab of 1H3 on the primary tumor model of B7x/4T1. 1H3 showed the superior efficacy to that of 1H3 Fab (Figure S4B). Taken together, these results suggest that 1H3 inhibits tumor growth through the combination of ADCC and functional neutralization of B7x.

DISCUSSION

Here we solved the structure of the functional IgV domain of B7x and developed a cancer immunotherapy targeting B7x. The B7 and CD28 families are very attractive therapeutic targets for human cancers. Compared to CTLA-4, PD-1 and PD-L1 that are targets for current clinical trials(Brahmer et al., 2012; Topalian et al., 2012), B7x has a very different expression pattern. In human, CTLA-4, PD-1, and PD-L1 are not expressed on resting T cells, but are induced after T cell activation and expressed on Tregs (Scandiuzzi et al., 2011). PD-1 and PD-L1 are induced on B cell, monocytes, and other immune cells after stimuli. By contrast, human B7x is hardly detected on immune cells even after stimulation (Lee et al., 2012). Neither CTLA-4 nor PD-1 are expressed on non-hematopoietic cells. PD-L1 is expressed on some normal tissues, whereas B7x is hardly detected in most human tissues (Choi et al., 2003). PD-L1 is expressed in some human cancers (Zang and Allison, 2007) whereas the expression of B7x in human cancers is more extensive including cancers of the esophagus (Chen et al., 2011), lung (Sun et al., 2006), breast (Tringler et al., 2005), pancreas (Awadallah et al., 2008), kidney (Krambeck et al., 2006), gut (Jiang et al., 2010), skin (Quandt et al., 2011), ovary (Zang et al., 2010)and prostate (Zang et al., 2007). Therefore, the expression pattern of B7x suggests that this target is more cancer specific.

The overall organization of the human B7x IgV domain is similar to that of other B7 family members (e.g., a structural alignment with PD-L1 is shown in Fig.1C). In addition to the secondary structure topology, conserved features include the disulfide bond connecting strands B and F (formed by Cys56 and Cys130) and the tryptophan residue (Trp71) at the domain core. The receptor-binding interface described for other B7 family members is located on the front-sheet surface of their IgV domains (Lazar-Molnar et al., 2008; Schwartz et al., 2001; Stamper et al., 2001). Thus, it is likely that B7x engages its receptor on the equivalent surface. Furthermore, our observation of a large branched glycan of the back-sheet of the B7x-IgV (linked to Asn112) would suggest that the back-sheet surface is unlikely to participate in receptor recognition. A glycosylation site at an equivalent position has been previously reported for murine B7-H3 ectodomain (Vigdorovich et al., 2013).

We demonstrated that mAbs against B7x achieved significant therapeutic efficacy in mouse cancer models. A new study also demonstrates that anti-B7x single-chain fragments variable (scFv) can delay OVCAR5 line growth in NSG mice(Dangaj et al., 2013). We and other

groups have previously shown that activated T cells express an unidentified receptor for B7x (Prasad et al., 2003; Sica et al., 2003; Zang et al., 2003) and our recent work reveal that MDSCs also have a receptor for B7x (Abadi et al., 2013). These results suggest that the expression of the B7x receptors is broader than previously thought. Due to the lack of the identity of B7x receptors, we developed an in vivo functional screen for anti-B7x mAbs. We found that the expression of B7x on CT26 tumor cells significantly promoted tumor progression in vivo, which mirrored clinical observations, and was used to validate therapeutic mAbs. 1H3 and 12D11 were found to reduce more than 60% of tumor nodules in lungs, with development of a strong immunologic memory in the case of 1H3. Similar results were obtained with the 4T1 tumor model.

Characterization of 1H3's binding properties showed that in addition to recognizing murine B7x, it also bound strongly to the IgV domain of human B7x and was able to significantly inhibit tumor nodules formation of human B7x-expressing CT26 in lungs. These results suggest that humanized 1H3 may prove useful in the treatment of human cancers. To advance this strategy, we mapped the epitopes recognized by 1H3 on human B7x using a series of mutants whose design was guided by the structure of B7x-IgV. The clustering of the antibody-blocking mutants to the "top" of the molecule, in particular, residues Ile62 and Lys63 in the BC loop of the back sheet and residue Ser135 in the FG loop of the front sheet, defines the minimal footprint for the B7x:1H3 binding interface. The combination of 1H3 functional blocking data and the mutagenesis data suggests that the binding surface for the physiologically relevant B7x receptor partially overlaps with this surface. Our results are consistent with observations that IgV domains predominately interact with other IgV domains via strands and a loop on their front sheets like is seen in the interactions between CTLA-4 and PD-1 and their ligands (Figure S5A–D)

It is surprising that 1H3 and 12D11 recognized similar epitopes in human B7x because 12D11 showed no in vivo suppressive effect on human B7x expressing CT26 cells. However, even though the difference was minor, 1H3 and 12D11 had at least one difference. Ile62 position in IgV domain of human B7x seemed to play significant roles in binding of B7x and anti-B7x mAbs. These results highlight the importance of our new in vivo screening system to find therapeutic mAbs against B7x.

The studies presented here suggest that the principal mechanisms of the anti-B7x mAb in dampening tumor progression are the neutralization of the B7x-mediated coinhibition of T cells and the ADCC-mediated direct killing of tumor cells. We demonstrated that 1H3 killed B7x-expressing tumor cells in a dose-dependent manner and that both 1H3 and its Fab fragment partially recovered T cell proliferation suppressed by B7x-Ig fusion protein. In line with these results, the Fab treatment significantly reduced lung tumor nodules, but its therapeutic efficacy was not as great as full 1H3 mAb treatment. These results suggest that both neutralization and ADCC may take place in vivo during the 1H3 treatment. The 1H3 treatment strongly increased the infiltration of major types of anti-tumor immune cells such as CD8 T cells including tumor antigen-specific CD8 T cells, NK cells, and IFN-γ-producing CD4 T cells. On the other hand, the treatment markedly reduced infiltration of immunosuppressive MDSCs. As a consequence, the treatment shifted the tumor microenvironment to a favorable anti-tumor state with a significantly higher ratio of effector

immune cells to the suppressive MDSCs and Tregs. Correspondingly, we found less VEGF and TGF-β in the tumor microenvironment after 1H3 treatment.

Therapies with mAbs against CTLA-4 and PD-1 target T cell coinhibitory receptors, whereas therapies with mAbs against PD-L1 and B7x target T cell coinhibitory ligands. The encouraging safety profile and anti-tumor activity from anti-PD-L1 clinical trial (Brahmer et al., 2012), together with preliminary data from anti-PD-1 trial that have suggested a correlation between tumor membrane PD-L1 expression and clinical response to anti-PD-1 antibodies (Topalian et al., 2012), highlight the emerging significance of targeting coinhibitory B7 ligands. Further studies with humanized anti-B7x antibodies, either as monotherapy or in synergism with traditional therapies, should be pursued for the treatment of human cancers.

EXPERIMENTAL PROCEDURES

Protein Crystallization and Structure Determination

Purified human B7x IgV protein was concentrated to 10 mg/mL in HBS-E (10 mM HEPES pH 7, 150 mM NaCl, 1 mM EDTA) and used to determine the initial crystallization conditions. Diffraction-quality crystals were obtained in 200 mM tri-Potassium citrate, 2.2 M ammonium sulfate, soaked in the well solution supplemented with 5-Amino-2,4,6 triiodo-isophthalic acid monohydrate (I3C) (Hampton Research) as a phasing reagent and 400 mM (final volume) lithium sulfate and flash-cooled in liquid nitrogen. Datasets at 1.075-Å and 1.54-Å wavelength were collected at the National Synchrotron Light Source beamline X29 (Upton, NY). Data were integrated using the iMosflm (Battye et al., 2011) with subsequent processing using the programs within the CCP4 software package (Winn et al., 2011). SAD phasing was carried out using the anomalous iodine (I3C) signal from a dataset collected at 1.54 Å and the initial electron density maps were obtained using SHELXC/D/E (Sheldrick, 2008) and HKL2MAP. Following initial model building using ARP/wARP (Langer et al., 2008), the model was refined using REFMAC5 (Murshudov et al., 1997) with further manual building using Coot (Emsley et al., 2010). Final coordinates and structure factors were deposited in Protein Databank and assigned PDB ID 4GOS

Animals and Human Tissues Slides

BALB/c mice were purchased from the National Cancer Institute (Fredrick, MD) and the Jackson Laboratory (Bar Harbor, ME). All mice were housed in a specific-pathogen-free facility. Human tumor tissue sections were obtained from IMEGENEX. All protocols were reviewed and approved by the Albert Einstein College of Medicine Institutional Animal Care and Use Committee and Institutional Review Board.

Monoclonal Antibodies against B7x and Generation of Fab Fragment

Hybridoma cells from 37G9, 12D11, 1H3 and 15D12 clones were maintained in serum free RPMI-1640 media(Wei et al., 2011). mAbs were purified on Protein G column (Thermo). Fractions of eluted mAbs were measured and pooled for buffer exchange to PBS via dialysis. Fab fragment preparation was performed based on manufacturer's protocol (Thermo).

Cell Lines and Tumors

CT26 and B7x/CT26 were cultured in RPMI-1640 containing 10% FBS, 100 U/ml penicillin, 100 μg/ml streptomycin, 2 mM L-glutamine, 1% nonessential amino acids and 1 mM sodium pyruvate. 4T1 and B7x/4T1 were cultured in DMEM supplemented with 10% FBS and 0.4 HSP U/ml insulin as described (Abadi et al., 2013). Eight to ten week old mice were iv injected with 10^5 cells in 0.2 ml DMEM. For survival studies of CT26 and B7x/CT26, 10^5 B7x/CT26 cells were iv injected into mice. Then survival rate was examined. For survival studies of 1H3 treatment, 10^4 B7x/CT26 cells were iv injected into mice, and same numbers of B7x/CT26 cells were injected for re-challenge. 10^5 B7x/4T1 cells were injected subcutaneously into the mammary fat pad of female mice for the primary tumor experiment. Tumor nodules on lungs were measures as previously described (Abadi et al., 2013).

Anti-B7x Immunotherapy

200 μg of mAbs against B7x, 1H3 Fab, or normal mouse IgG were ip injected at days 1, 3, 7, 11, and 14. Each mouse received a total of 1mg of antibody or Fab during B7x/CT26 experiments. At day 17, mice were sacrificed for counting tumor nodules in lungs. For hB7x/CT26 experiments, 200μg of mAbs against B7x (1H3 and 12D11), or normal mouse IgG were ip injected at days 1, 2, 3, 5, 7, 9, 11, 13, and 15. Each mouse received total 1.8mg antibody. At day 17, mice were sacrificed for counting tumor nodules in lungs. For the B7x/4T1 primary tumor model, one week after tumor injection, mice were grouped based on their tumor volume. 300μg of mAbs were ip injected at days 8,11,13,15, and 18. Tumor volume was measured every two or three days after 7 days. At day 20, mice were sacrificed, breast tumors were excised and weighed, and tumor nodules on lungs were counted.

Human B7x mutagenesis and epitope mapping

Ectodomain of hB7x (Gly21 – Ala208) was cloned into a type I secretion ligation independent cloning vector we designed in house. Cloning into this vector fuses the target ectodomain to a non-native transmembrane domain (TM domain from murine PD-L1) followed by the mCherry protein (as a cytosolic expression proxy). We have successfully used this vector to study expression, localization and activity of several other members of the IgG superfamily. The wild-type hB7x type I secretion construct was transfected into HEK 293S cells. Cell surface expression of B7x was confirmed by FACS analysis using the B7x-specific mAb 1H3. Residues for site-directed mutagenesis were initially selected on the basis of our crystal structure of the hB7x-IgV domain to identify surface exposed residues within the IgV domain. Surface exposed residues clearly involved in a salt-bridge were omitted from the set of targeted residues. Mutagenesis was performed using a standard PCR method using high fidelity KOD polymerase. All of the successful mutants were sequence-verified and individually transfected into HEK293S cells using 24-well suspension plates. Two days post-transfection the cells were counted and diluted to 1×10^6 cells/mL using 1x PBS with 2% BSA. 0.2×10^6 cells were incubated with 2 μg of the 1H3 mAb for 1 hour at 4°C. Cells were subsequently pelleted by centrifugation at 500×g and washed with PBS for a total of three times. Goat anti-mouse DyLight 488 secondary antibody (2 μg) was added to the cells and they were incubated at 4°C for 45 min. Cells were washed and antibody binding was assessed by FACS analysis on a BD Aria III. Flow cytometry data were gated

for all mCherry positive events (hB7x expression) and then sub-gated for anti-B7x binding (488 channel). To consider slight variation in total expression of each mutant the number of antibody bound events was divided by the total number of mCherry-positive events. The experiment was performed in duplicate.

Statistics

Statistical analysis was performed with Prism software (Graphpad) using the unpaired Student *t*-test or the log-rank test (Mantel-Cox) for the survival study. P values of < 0.05 were considered statistically significant.

Supplementary Material

Refer to Web version on PubMed Central for supplementary material.

Acknowledgments

This work was supported by NIH R01CA175495 and DOD PC131008 (X.Z.), NIH GM094662 and GM094665 (S.C.A.), UL1TR000086 (M.J.), F31CA183493 (K.C.O.) and T32GM007288 (J.M.C.). We also acknowledge support from the Albert Einstein Cancer Center (P30CA013330), Diabetes Research Center (P60DK020541), Center for AIDS Research (AI51519) and Institute for Aging Research (P30AG038072).

References

Abadi YM, Jeon H, Ohaegbulam KC, Scandiuzzi L, Ghosh K, Hofmeyer KA, Lee JS, Ray A, Gravekamp C, Zang X. Host b7x promotes pulmonary metastasis of breast cancer. J Immunol. 2013; 190:3806–3814. [PubMed: 23455497]

Aslakson CJ, Miller FR. Selective events in the metastatic process defined by analysis of the sequential dissemination of subpopulations of a mouse mammary tumor. Cancer Res. 1992; 52:1399–1405. [PubMed: 1540948]

Awadallah NS, Shroyer KR, Langer DA, Torkko KC, Chen YK, Bentz JS, Papkoff J, Liu W, Nash SR, Shah RJ. Detection of B7-H4 and p53 in pancreatic cancer: potential role as a cytological diagnostic adjunct. Pancreas. 2008; 36:200–206. [PubMed: 18376314]

Barach YS, Lee JS, Zang X. T cell coinhibition in prostate cancer: new immune evasion pathways and emerging therapeutics. Trends Mol Med. 2010

Battye TG, Kontogiannis L, Johnson O, Powell HR, Leslie AG. iMOSFLM: a new graphical interface for diffraction-image processing with MOSFLM. Acta Crystallogr D Biol Crystallogr. 2011; 67:271–281. [PubMed: 21460445]

Brahmer JR, Tykodi SS, Chow LQ, Hwu WJ, Topalian SL, Hwu P, Drake CG, Camacho LH, Kauh J, Odunsi K, et al. Safety and activity of anti-PD-L1 antibody in patients with advanced cancer. N Engl J Med. 2012; 366:2455–2465. [PubMed: 22658128]

Chen LJ, Sun J, Wu HY, Zhou SM, Tan Y, Tan M, Shan BE, Lu BF, Zhang XG. B7-H4 expression associates with cancer progression and predicts patient's survival in human esophageal squamous cell carcinoma. Cancer Immunol Immunother. 2011; 60:1047–1055. [PubMed: 21519829]

Choi IH, Zhu G, Sica GL, Strome SE, Cheville JC, Lau JS, Zhu Y, Flies DB, Tamada K, Chen L. Genomic organization and expression analysis of B7-H4, an immune inhibitory molecule of the B7 family. J Immunol. 2003; 171:4650–4654. [PubMed: 14568939]

Clynes RA, Towers TL, Presta LG, Ravetch JV. Inhibitory Fc receptors modulate in vivo cytotoxicity against tumor targets. Nat Med. 2000; 6:443–446. [PubMed: 10742152]

Dangaj D, Lanitis E, Zhao A, Joshi S, Cheng Y, Sandaltzopoulos R, Ra HJ, Danet-Desnoyers G, Powell DJ Jr. Scholler N. Novel recombinant human b7-h4 antibodies overcome tumoral immune escape to potentiate T-cell antitumor responses. Cancer Res. 2013; 73:4820–4829. [PubMed: 23722540]

Emsley P, Lohkamp B, Scott WG, Cowtan K. Features and development of Coot. Acta Crystallogr D Biol Crystallogr. 2010; 66:486–501. [PubMed: 20383002]

Fiocco U, Sfriso P, Oliviero F, Pagnin E, Scagliori E, Campana C, Dainese S, Cozzi L, Punzi L. Co-stimulatory modulation in rheumatoid arthritis: the role of (CTLA4-Ig) abatacept. Autoimmun Rev. 2008; 8:76–82. [PubMed: 18718877]

Fourcade J, Sun Z, Benallaoua M, Guillaume P, Luescher IF, Sander C, Kirkwood JM, Kuchroo V, Zarour HM. Upregulation of Tim-3 and PD-1 expression is associated with tumor antigen-specific CD8+ T cell dysfunction in melanoma patients. J Exp Med. 2010; 207:2175–2186. [PubMed: 20819923]

Fridlender ZG, Sun J, Kim S, Kapoor V, Cheng G, Ling L, Worthen GS, Albelda SM. Polarization of tumor-associated neutrophil phenotype by TGF-beta: "N1" versus "N2" TAN. Cancer Cell. 2009; 16:183–194. [PubMed: 19732719]

Goding SR, Wilson KA, Xie Y, Harris KM, Baxi A, Akpinarli A, Fulton A, Tamada K, Strome SE, Antony PA. Restoring immune function of tumor-specific CD4+ T cells during recurrence of melanoma. J Immunol. 2013; 190:4899–4909. [PubMed: 23536636]

Greenwald RJ, Freeman GJ, Sharpe AH. The B7 family revisited. Annu Rev Immunol. 2005; 23:515–548. [PubMed: 15771580]

Hodi FS, O'Day SJ, McDermott DF, Weber RW, Sosman JA, Haanen JB, Gonzalez R, Robert C, Schadendorf D, Hassel JC, et al. Improved survival with ipilimumab in patients with metastatic melanoma. N Engl J Med. 2010; 363:711–723. [PubMed: 20525992]

Hofmeyer KA, Scandiuzzi L, Ghosh K, Pirofski LA, Zang X. Tissue-expressed B7x affects the immune response to and outcome of lethal pulmonary infection. J Immunol. 2012; 189:3054–3063. [PubMed: 22855708]

Huang AY, Gulden PH, Woods AS, Thomas MC, Tong CD, Wang W, Engelhard VH, Pasternack G, Cotter R, Hunt D, et al. The immunodominant major histocompatibility complex class I-restricted antigen of a murine colon tumor derives from an endogenous retroviral gene product. Proc Natl Acad Sci U S A. 1996; 93:9730–9735. [PubMed: 8790399]

Isitman G, Stratov I, Kent SJ. Antibody-Dependent Cellular Cytotoxicity and NK Cell-Driven Immune Escape in HIV Infection: Implications for HIV Vaccine Development. Adv Virol. 2012; 2012:637208. [PubMed: 22611395]

Janakiram M, Abadi YM, Sparano JA, Zang X. T cell coinhibition and immunotherapy in human breast cancer. Discov Med. 2012; 14:229–236. [PubMed: 23114578]

Janakiram M, Chinai JC, Fineberg S, Fiser A, Montagna C, Madaverepu R, Castano E, Jeon H, Ohaegbulam KC, Zhao R, Zhao A, Almo SC, Sparano JC, Zang X. Expression, clinical significance, and receptor identification of the newest B7 family member HHLA2 protein. Clin Cancer Res. 2014

Jeon H, Ohaegbulam KC, Abadi YM, Zang X. B7x and myeloid-derived suppressor cells in the tumor microenvironment: A tale of two cities. Oncoimmunology. 2013; 2:e24744. [PubMed: 24073367]

Jiang J, Zhu Y, Wu C, Shen Y, Wei W, Chen L, Zheng X, Sun J, Lu B, Zhang X. Tumor expression of B7-H4 predicts poor survival of patients suffering from gastric cancer. Cancer Immunol Immunother. 2010; 59:1707–1714. [PubMed: 20725832]

Kohrt HE, Houot R, Marabelle A, Cho HJ, Osman K, Goldstein M, Levy R, Brody J. Combination strategies to enhance antitumor ADCC. Immunotherapy. 2012; 4:511–527. [PubMed: 22642334]

Krambeck AE, Thompson RH, Dong H, Lohse CM, Park ES, Kuntz SM, Leibovich BC, Blute ML, Cheville JC, Kwon ED. B7-H4 expression in renal cell carcinoma and tumor vasculature: associations with cancer progression and survival. Proc Natl Acad Sci U S A. 2006; 103:10391–10396. [PubMed: 16798883]

Langer G, Cohen SX, Lamzin VS, Perrakis A. Automated macromolecular model building for X-ray crystallography using ARP/wARP version 7. Nat Protoc. 2008; 3:1171–1179. [PubMed: 18600222]

Lazar-Molnar E, Yan Q, Cao E, Ramagopal U, Nathenson SG, Almo SC. Crystal structure of the complex between programmed death-1 (PD-1) and its ligand PD-L2. Proc Natl Acad Sci U S A. 2008; 105:10483–10488. [PubMed: 18641123]

Lee JS, Scandiuzzi L, Ray A, Wei J, Hofmeyer KA, Abadi YM, Loke P, Lin J, Yuan J, Serreze DV, et al. B7x in the periphery abrogates pancreas-specific damage mediated by self-reactive CD8 T cells. J Immunol. 2012; 189:4165–4174. [PubMed: 22972920]

Lin DY, Tanaka Y, Iwasaki M, Gittis AG, Su HP, Mikami B, Okazaki T, Honjo T, Minato N, Garboczi DN. The PD-1/PD-L1 complex resembles the antigen-binding Fv domains of antibodies and T cell receptors. Proc Natl Acad Sci U S A. 2008; 105:3011–3016. [PubMed: 18287011]

Murshudov GN, Vagin AA, Dodson EJ. Refinement of macromolecular structures by the maximum-likelihood method. Acta Crystallogr D Biol Crystallogr. 1997; 53:240–255. [PubMed: 15299926]

Prasad DV, Richards S, Mai XM, Dong C. B7S1, a novel B7 family member that negatively regulates T cell activation. Immunity. 2003; 18:863–873. [PubMed: 12818166]

Quandt D, Fiedler E, Boettcher D, Marsch W, Seliger B. B7-h4 expression in human melanoma: its association with patients' survival and antitumor immune response. Clin Cancer Res. 2011; 17:3100–3111. [PubMed: 21378130]

Roda JM, Wang Y, Sumner LA, Phillips GS, Marsh CB, Eubank TD. Stabilization of HIF-2alpha induces sVEGFR-1 production from tumor-associated macrophages and decreases tumor growth in a murine melanoma model. J Immunol. 2012; 189:3168–3177. [PubMed: 22869907]

Roland CL, Lynn KD, Toombs JE, Dineen SP, Udugamasooriya DG, Brekken RA. Cytokine levels correlate with immune cell infiltration after anti-VEGF therapy in preclinical mouse models of breast cancer. PLoS One. 2009; 4:e7669. [PubMed: 19888452]

Scandiuzzi L, Ghosh K, Zang X. T cell costimulation and coinhibition: genetics and disease. Discov Med. 2011; 12:119–128. [PubMed: 21878189]

Schwartz JC, Zhang X, Fedorov AA, Nathenson SG, Almo SC. Structural basis for co-stimulation by the human CTLA-4/B7-2 complex. Nature. 2001; 410:604–608. [PubMed: 11279501]

Sharma P, Wagner K, Wolchok JD, Allison JP. Novel cancer immunotherapy agents with survival benefit: recent successes and next steps. Nat Rev Cancer. 2011; 11:805–812. [PubMed: 22020206]

Sheldrick GM. A short history of SHELX. Acta Crystallogr A. 2008; 64:112–122. [PubMed: 18156677]

Sica GL, Choi IH, Zhu G, Tamada K, Wang SD, Tamura H, Chapoval AI, Flies DB, Bajorath J, Chen L. B7-H4, a molecule of the B7 family, negatively regulates T cell immunity. Immunity. 2003; 18:849–861. [PubMed: 12818165]

Stamper CC, Zhang Y, Tobin JF, Erbe DV, Ikemizu S, Davis SJ, Stahl ML, Seehra J, Somers WS, Mosyak L. Crystal structure of the B7-1/CTLA-4 complex that inhibits human immune responses. Nature. 2001; 410:608–611. [PubMed: 11279502]

Sun Y, Wang Y, Zhao J, Gu M, Giscombe R, Lefvert AK, Wang X. B7-H3 and B7-H4 expression in non-small-cell lung cancer. Lung Cancer. 2006; 53:143–151. [PubMed: 16782226]

Topalian SL, Hodi FS, Brahmer JR, Gettinger SN, Smith DC, McDermott DF, Powderly JD, Carvajal RD, Sosman JA, Atkins MB, et al. Safety, activity, and immune correlates of anti-PD-1 antibody in cancer. N Engl J Med. 2012; 366:2443–2454. [PubMed: 22658127]

Tringler B, Zhuo S, Pilkington G, Torkko KC, Singh M, Lucia MS, Heinz DE, Papkoff J, Shroyer KR. B7-h4 is highly expressed in ductal and lobular breast cancer. Clin Cancer Res. 2005; 11:1842–1848. [PubMed: 15756008]

Vigdorovich V, Ramagopal UA, Lazar-Molnar E, Sylvestre E, Lee JS, Hofmeyer KA, Zang X, Nathenson SG, Almo SC. Structure and T cell inhibition properties of B7 family member, B7-H3. Structure. 2013; 21:707–717. [PubMed: 23583036]

Vincenti F, Dritselis A, Kirkpatrick P. Belatacept. Nat Rev Drug Discov. 2011; 10:655–656. [PubMed: 21878974]

Wei J, Loke P, Zang X, Allison JP. Tissue-specific expression of B7x protects from CD4 T cell-mediated autoimmunity. J Exp Med. 2011; 208:1683–1694. [PubMed: 21727190]

Winn MD, Ballard CC, Cowtan KD, Dodson EJ, Emsley P, Evans PR, Keegan RM, Krissinel EB, Leslie AG, McCoy A, et al. Overview of the CCP4 suite and current developments. Acta Crystallogr D Biol Crystallogr. 2011; 67:235–242. [PubMed: 21460441]

Zang X, Allison JP. The B7 family and cancer therapy: costimulation and coinhibition. Clin Cancer Res. 2007; 13:5271–5279. [PubMed: 17875755]

Zang X, Loke P, Kim J, Murphy K, Waitz R, Allison JP. B7x: a widely expressed B7 family member that inhibits T cell activation. Proceedings of the National Academy of Sciences of the United States of America. 2003; 100:10388–10392. [PubMed: 12920180]

Zang X, Sullivan PS, Soslow RA, Waitz R, Reuter VE, Wilton A, Thaler HT, Arul M, Slovin SF, Wei J, et al. Tumor associated endothelial expression of B7-H3 predicts survival in ovarian carcinomas. Mod Pathol. 2010; 23:1104–1112. [PubMed: 20495537]

Zang X, Thompson RH, Al-Ahmadie HA, Serio AM, Reuter VE, Eastham JA, Scardino PT, Sharma P, Allison JP. B7-H3 and B7x are highly expressed in human prostate cancer and associated with disease spread and poor outcome. Proc Natl Acad Sci U S A. 2007; 104:19458–19463. [PubMed: 18042703]

Zhao R, Chinai JM, Buhl S, Scandiuzzi L, Ray A, Jeon H, Ohaegbulam KC, Ghosh K, Zhao A, Scharff MD, et al. HHLA2 is a member of the B7 family and inhibits human CD4 and CD8 T-cell function. Proc Natl Acad Sci U S A. 2013; 110:9879–9884. [PubMed: 23716685]

Zhou Q, Munger ME, Veenstra RG, Weigel BJ, Hirashima M, Munn DH, Murphy WJ, Azuma M, Anderson AC, Kuchroo VK, et al. Coexpression of Tim-3 and PD-1 identifies a CD8+ T-cell exhaustion phenotype in mice with disseminated acute myelogenous leukemia. Blood. 2011; 117:4501–4510. [PubMed: 21385853]

Zhu Y, Yao S, Iliopoulou BP, Han X, Augustine MM, Xu H, Phennicie RT, Flies SJ, Broadwater M, Ruff W, et al. B7-H5 costimulates human T cells via CD28H. Nat Commun. 2013; 4:2043. [PubMed: 23784006]

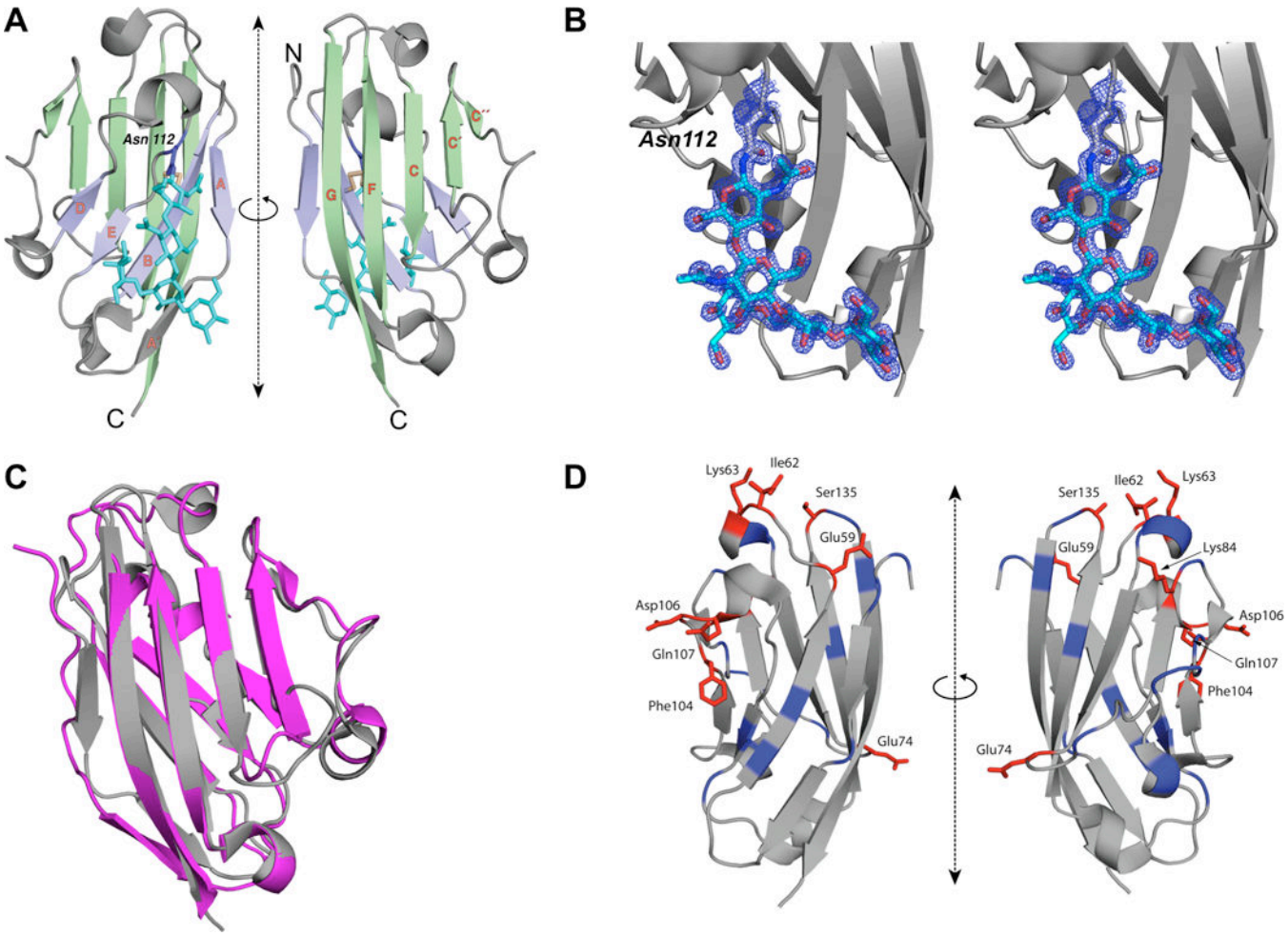

Figure 1. The Structure of Human B7x IgV Domain and the Epitopes Recognized by Monoclonal Antibody against B7x

(A) Ribbon representation of the structure of human B7x-IgV (front-sheet: light green, back-sheet: light purple, disulfide: light yellow) is shown in two orientations. The strands of the β-sandwich are labeled in orange; the side chain of Asn112 (purple) and the N-linked glycan (cyan) are shown in stick-figure representation. (B) Electron density observed near Asn112 corresponds to an N-linked glycan. Ribbon representation of the structure of human B7x-IgV (gray) is shown. Electron density map ($2F_o–F_c$), contoured at +2σ, and covering the area near and including Asn112 is shown in mesh representation (blue). The 5 residues of N-linked glycan are shown in stick representation. (C) Superposition of B7x and PD-L1. Gray represents IgV domain of human PD-L1 and Pink represents IgV domain of human B7x. (D) Ribbon diagram of the IgV domain of B7x showing the location of residues targeted for mutagenesis. Positions that when mutated resulted in at least 40% reduction in 1H3 binding are highlighted in red, while the remainder of targeted positions are highlighted in blue.

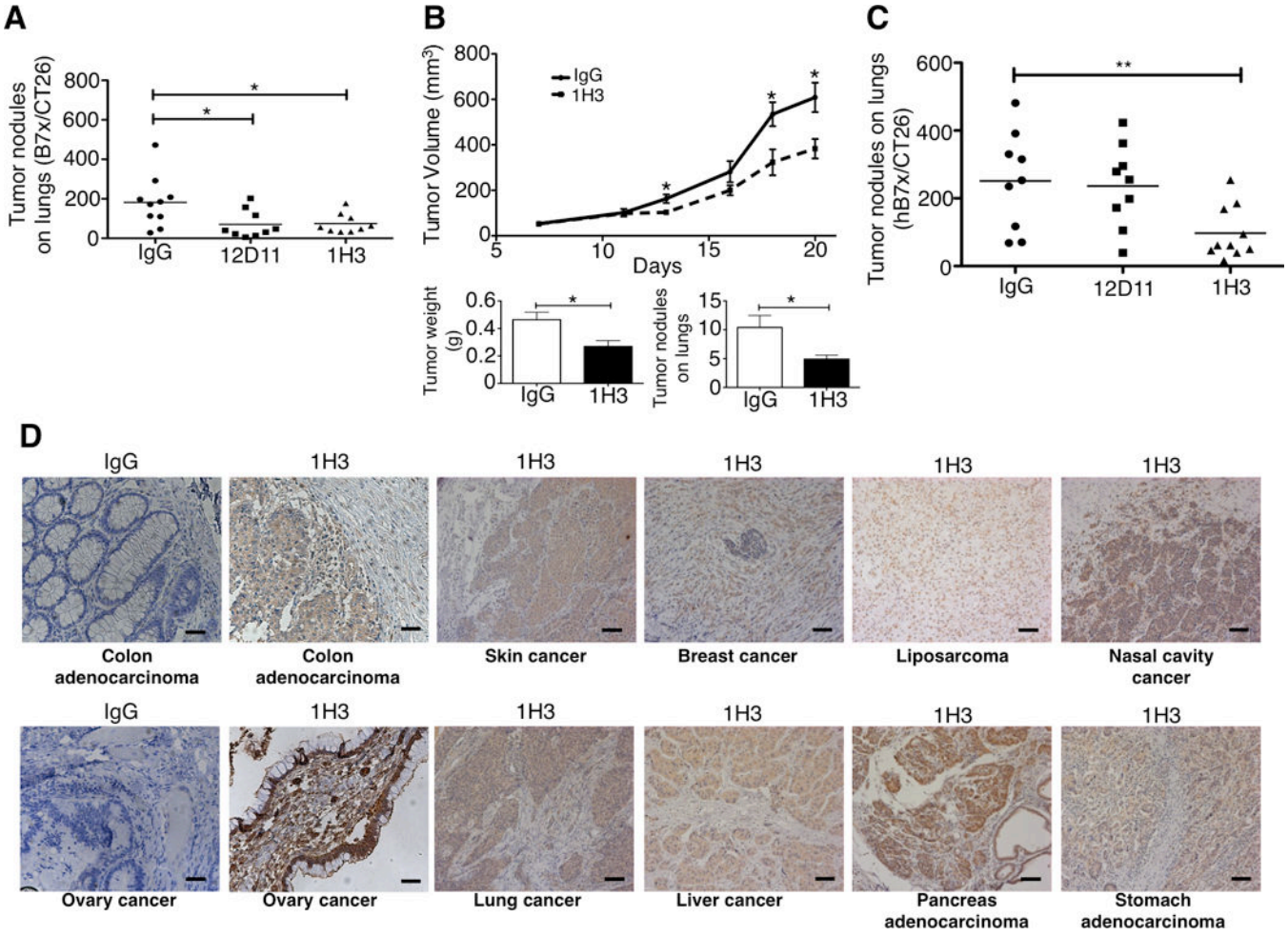

Figure 2. Effect of Anti-B7x Monoclonal Antibodies on Tumor Growth

(A) BALB/c mice were iv injected with B7x/CT26 then with anti-B7x mAbs 12D11 and 1H3 or mouse IgG. After sacrifice, tumor nodules in lungs were counted. Data were pooled from three independent experiments (n= 9 or 10). (B) BALB/c females were injected with B7x/4T1 in the mammary fat pad. Mice were ip treated with mAb 1H3. Tumor volumes were measured every two or three days after tumor injection. After mice were sacrificed, tumor weights were measured and tumor nodules on lungs were counted (n=10). *$p<0.05$. (C) BALB/c mice were iv injected with CT26 cells expressing human B7x (hB7x/CT26) and then injected ip with mAb 1H3 or control IgG. After sacrificing the mice, tumor nodules in the lungs were counted (n=9). Results were pooled from two independent experiments. (D) Several human cancers were stained with 1H3 or IgG control using immunohistochemistry. Bars 50μm.

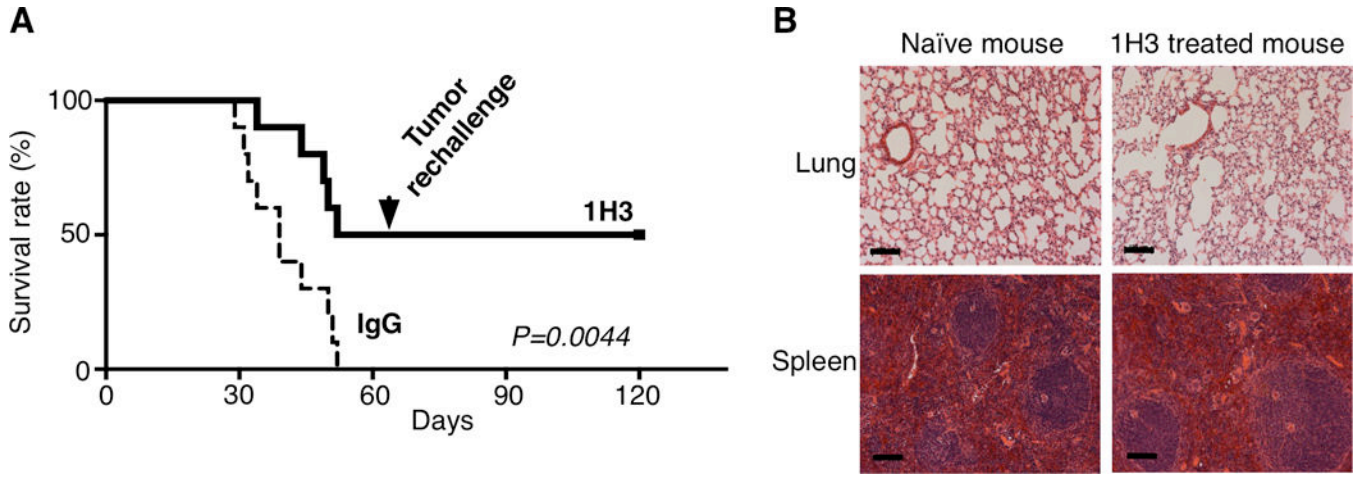

Figure 3. Effect of Anti-B7x Therapy on Survival and Tumor Rechallenge

(A) BALB/c mice were iv injected with B7x/CT26 at day 0 and then injected ip with 1H3 or control IgG. At day 60 post-injection, the surviving mice were iv rechallenged with B7x/CT26 (n=10). *p<0.05; **p<0.01. (B) At day 120, surviving mice were sacrificed and lung sections were used for HE staining. Representative lung tissues from surviving and naïve mice are shown. Bar 100μm.

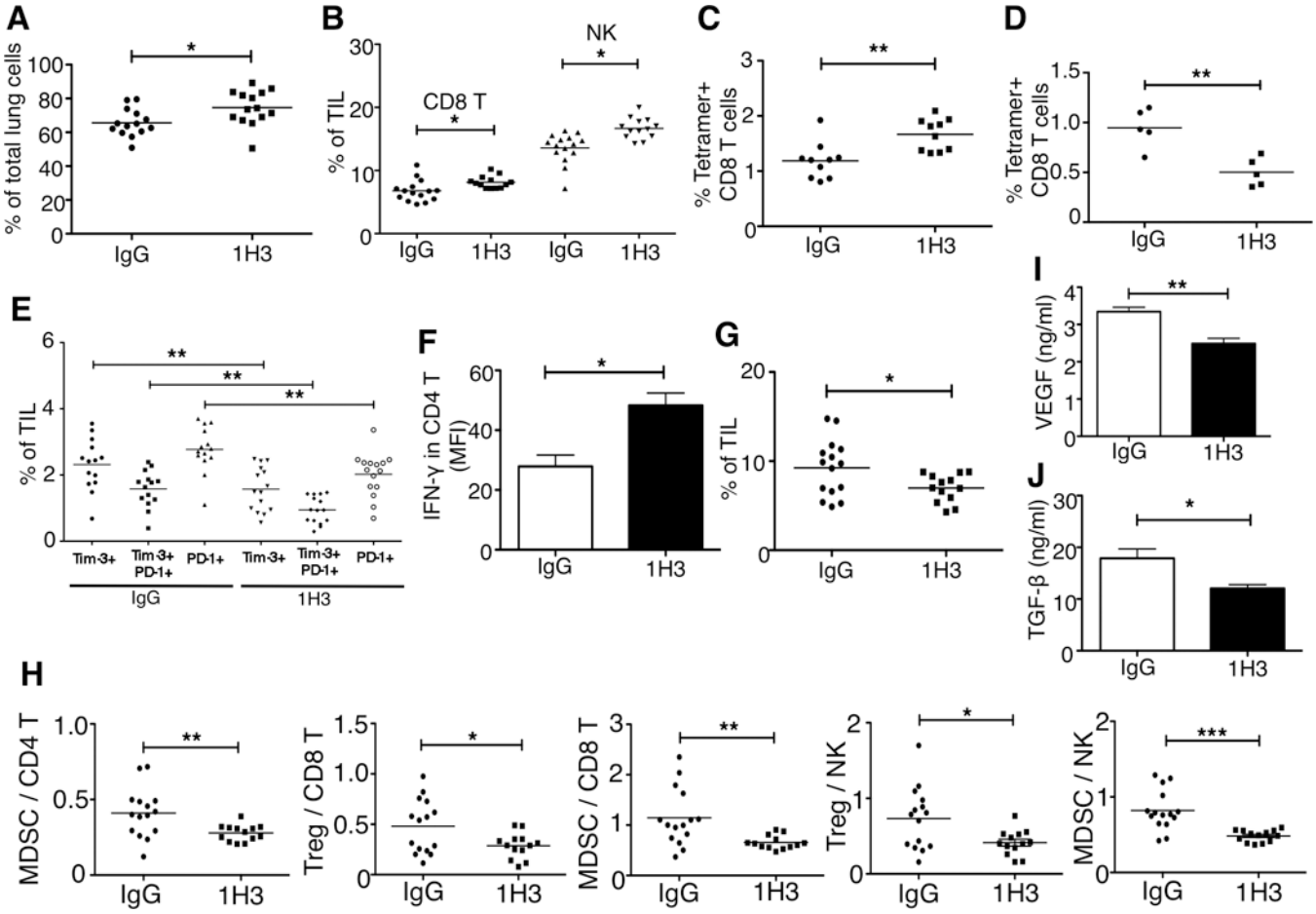

Figure 4. Anti-B7x Therapy Alters the Intratumor Balance of Anti-tumor Effector Immune Cells and Immunosuppressive Cells

BALB/c mice were iv injected with B7x/CT26 and then treated with 1H3 or control mouse IgG. At day 17, single-cell suspensions from tumor bearing lungs were analyzed by FACS for the percentage of infiltrated CD45+ cells (A), the percentage of CD8 T cells and NK cells (B), the percentage of tumor antigen AH1 (SPSYVYHQF)-specific CD8 T cells (C), the percentage of CD4 T cells that were Tim-3+PD-1+, Tim-3+ alone and PD-1+ alone (E), and CD11b+Ly6C+ monocytic myeloid-derived suppressor cells (G). At day 17, single-cell suspensions from bloods were analyzed by FACS for the percentage of tumor antigen AH1-specific CD8+ T cells were measured (D). Cell suspensions from tumor bearing lungs were stimulated with 1x cell stimulation cocktail for 5 hours and stained with antibodies to CD3, CD4 and IFN-γ or isotype controls (F). Results are pooled from three independent experiments; *p<0.05, **p<0.01. Result of (D) is a representative data from two independent experiments. (H) The ratios of Treg (Foxp3+ CD4+) and MDSCs to CD8 T cells, CD4 T cells, and NK cells. These results are pooled from three independent experiments; *p<0.05, **p<0.01, ***p<0.001. (I) Total amount of VEGF from tumor bearing lungs was measured using ELISA. **p<0.01. (J) Total amount of TGF-β from tumor bearing lungs were measured using ELISA. Each group contained 5 mice. *p<0.05.

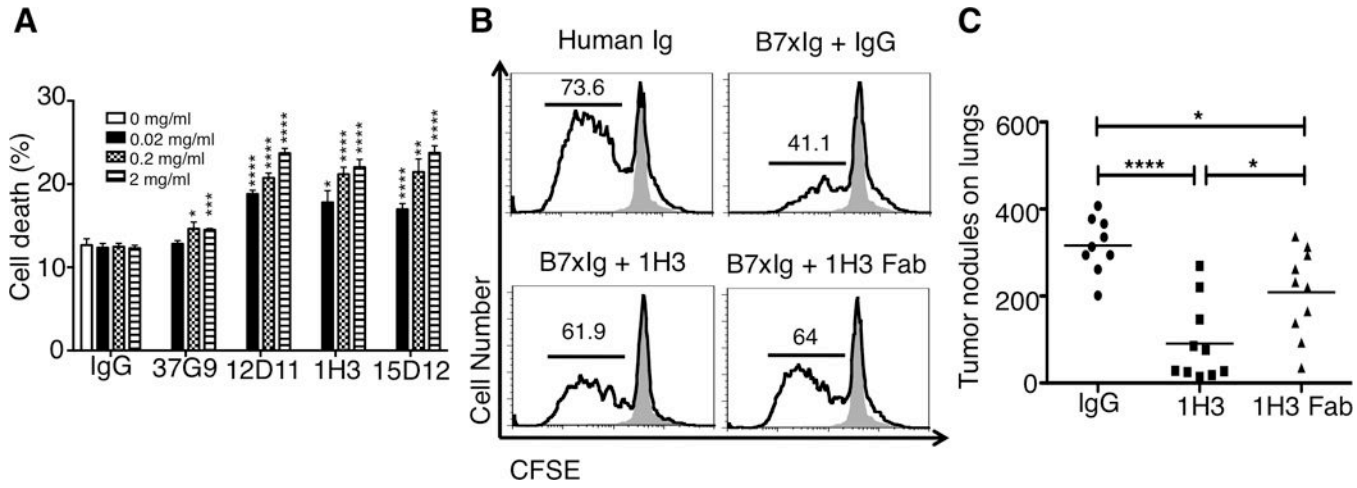

Figure 5. Anti-tumor Mechanisms of 1H3 Treatment

(A) mAbs against B7x killed CT26 tumor cells expressing B7x through antibody-dependent cellular cytotoxicity in vitro. Data are representative of two independent experiments in triplicates and shown as mean ± SE. **p<0.01; ****p<0.0001. (B) 1H3 partially neutralized B7x-mediated T cell coinhibition. CFSE-labeled T cells were incubated for four days with plate-bound anti-CD3 in the presence of control Ig, B7x-Ig and IgG (2 μg/ml), B7x-Ig and 1H3 (2 μg/ml), or B7x-Ig and 1H3 Fab (4 μg/ml). Representative FACS plots show CFSE dilution among live stimulated cells (solid line) compared to unstimulated control T cells (shaded area). Data are representative of two independent experiments. (C) Comparison of therapeutic efficacies between 1H3 and its Fab. Data were pooled from two independent experiments (n=9 or 10). *p<0.05; **p<0.01, ***p<0.001, ****p<0.0001.

Table 1

Data Collection, Phasing and Refinement Statistics (SAD)

Data collection	***native***	***I3C***
Space group	P 4_32_12	P 4_32_12
Cell dimensions		
a, *b*, *c* (Å)	46.5, 46.5, 115.77	46.47, 46.47, 116.15
a, b, g (°)	90, 90, 90	90, 90, 90
Wavelength	1.075	1.5402
Resolution (Å)	43.1–1.59	38.72–1.79
R_{sym} or R_{merge}	8.8 (48.9)	16.1 (179)
I / sI	17.7 (1.6)	13.8 (1.8)
Completeness (%)	90.1 (100.0)	86.4 (89.4)
Redundancy	13.3 (13.5)	18.4 (19.7)
Refinement		
Resolution (Å)	1.59	
No. reflections	15194	
R_{work} / R_{free}	17.4 (23.2) / 19.2 (22.6)	
No. atoms		
Protein	871	
Ligand/ion	61	
Water	111	
B-factors		
Protein	15.0	
Ligand/ion	13.8	
Water	24.1	
R.m.s deviations		
Bond lengths (Å)	0.009	
Bond angles (°)	1.474	

One crystal was used for native and one for I3C-derivatized datasets.

Values in parentheses are for highest-resolution shell.

Table 2

Surface Plasmon Resonance Measurements.

murine B7x (IgV domain)			
mAb	k_{on} ($M^{-1}{\cdot}s^{-1}$)	k_{off} (s^{-1})	K_D (nM)
1H3	2.455(4)[a]×10^6	0.001248(7)	0.508(3)
12D11	2.140(4)×10^6	0.001341(8)	0.627(4)
15D12	1.790(3)×10^6	0.001135(7)	0.634(4)
murine B7x			
mAb	k_{on} ($M^{-1}{\cdot}s^{-1}$)	k_{off} (s^{-1})	K_D (nM)
1H3	6.71(3)×10^5	0.001298(7)	1.94(1)
12D11	6.62(4)×10^5	0.001177(7)	1.78(1)
15D12	4.40(3)×10^5	0.001095(6)	2.49(2)
human B7x (IgV domain)			
mAb	k_{on} ($M^{-1}{\cdot}s^{-1}$)	k_{off} (s^{-1})	K_D (nM)
1H3	2.53(2)×10^5	0.00917(4)	36.2(3)
12D11	2.13(1)×10^5	0.00928(3)	43.5(3)
15D12	1.388(7)×10^5	0.01039(2)	74.9(4)

[a]The value in parentheses denotes the standard error in the last digit